ELSEVIER

Comput. Methods Appl. Mech. Engrg. 191 (2002) 1491–1503

Computer methods in applied mechanics and engineering

www.elsevier.com/locate/cma

Higher order stabilized finite element method for hyperelastic finite deformation

Antoinette M. Maniatty *, Yong Liu, Ottmar Klaas, Mark S. Shephard

Department of Mechanical Engineering, Aeronautical Engineering & Mechanics and Scientific Computation Research Center, Rensselaer Polytechnic Institute, Troy, NY 12180, USA

Received 23 March 2001; received in revised form 30 July 2001

Abstract

This paper presents a higher order stabilized finite element formulation for hyperelastic large deformation problems involving incompressible or nearly incompressible materials. A Lagrangian finite element formulation is presented where mesh dependent terms are added element-wise to enhance the stability of the mixed finite element formulation. A reconstruction method based on local projections is used to compute the higher order derivatives that arise in the stabilization terms, specifically derivatives of the stress tensor. Linearization of the weak form is derived to enable a Newton–Raphson solution procedure of the resulting non-linear equations. Numerical experiments using the stabilization method with equal order shape functions for the displacement and pressure fields in hyperelastic problems show that the stabilized method is effective for some non-linear finite deformation problems. Finally, conclusions are inferred and extensions of this work are discussed.

Keywords: Hyperelasticity; Stabilized finite element method; Finite deformation

1. Introduction

Stabilized finite element methods (SFEMs) consist of adding mesh dependent terms to the usual Galerkin method (see, for example, the works of [1,2]) in order to improve the stability of the solution in problems with known instabilities, for example in modeling incompressible material deformation. Without the added stabilization terms, Galerkin methods applied to incompressible or nearly incompressible material behavior in the setting of a mixed finite element method must fulfill the Ladyzenskaya–Babuska–Brezzi (LBB) condition to achieve unique solvability, convergence and robustness [3]. This places severe restrictions on the choice of the solution space. Without balancing the interpolation functions according to the LBB condition, large errors or oscillations may appear in the solution. Furthermore, the LBB condition complicates the use of *p*-adaptive techniques, where flexibility is needed in varying the interpolation order. The advantage of stabilized methods is that they do not impose constraints on the interpolation functions, thus allowing for greater flexibility in balancing efficiency and accuracy.

SFEMs, which avoid the limitations on the interpolation functions in the traditional Galerkin finite element method, are widely used now, especially in applications in fluid mechanics. The stabilization terms, which are added to the usual Galerkin formulation, are functions of the residuals of the Euler–Lagrange equations evaluated element-wise. From the construction, it follows that consistency is not affected since the exact solution satisfies both the Galerkin term and the additional terms (see, for example, the works of [1,4,5]). Recently, Klaas et al. [6] have applied a stabilized finite element method with linear elements to

* Corresponding author. Tel.: +1-518-276-6984; fax: +1-518-276-6025.
E-mail address: maniaa@rpi.edu (A.M. Maniatty).

0045-7825/02/$ - see front matter
PII: S0045-7825(01)00335-8

hyperelasticity, and the results show the effectiveness of the stabilized finite element method for large deformation problems. However, higher order stabilized finite elements were not implemented in that work because of the difficulty in computing the required higher order derivatives.

In this paper, a higher order stabilized finite element formulation in a Lagrangian reference frame for hyperelasticity is developed. A Petrov–Galerkin method, following that presented in [1], is used. This results in a term with the strong form of the equilibrium equation being added to the usual Galerkin method. This term involves the divergence of part of the stress tensor, which, in turn, depends on the deformation gradient field. In this work, a local reconstruction method, following the work presented for two-dimensional Navier–Stokes equations in [7], is used to compute the stress at the finite element nodal locations. Then the divergence of the reconstructed stress is computed from the nodal quantities and shape functions. Numerical examples with a non-linear hyperelastic constitutive law for rubber-like materials are given. Finally, conclusions are inferred and directions for future work are discussed.

2. Governing equations for Lagrangian description

Consider a three-dimensional reference domain B with boundary Γ. The boundary value problem for finite elasticity in the absence of body forces defined on the reference configuration is given as

Find a displacement field $\mathbf{u}$ such that

$$\mathrm{Div}\,(\mathbf{FS}) = 0 \quad \text{in } B \tag{1}$$

with boundary conditions

$$(\mathbf{FS})\mathbf{n} = \mathbf{g} \quad \text{on } \Gamma_N, \tag{2}$$

$$\mathbf{u} = \bar{\mathbf{u}} \quad \text{on } \Gamma_D, \tag{3}$$

where $\mathbf{F}$ is the deformation gradient, $\mathbf{S}$ is the second Piola–Kirchoff stress, $\mathbf{n}$ is the outward unit normal and $\mathbf{g}$ is the prescribed traction load on Γ_N, and $\bar{\mathbf{u}}$ is the prescribed displacement on Γ_D. Finally, for completeness, the boundary conditions must be specified on the entire boundary for each degree of freedom without overlap, so on a component by component basis $\Gamma_N \cup \Gamma_D = \Gamma$, $\Gamma_N \cap \Gamma_D = \emptyset$.

We assume a hyperelastic, homogeneous material behavior for which a free energy function, W, a function of the Cauchy–Green tensor $\mathbf{C} = \mathbf{F}^{\mathrm{T}}\mathbf{F}$, exists. The standard additive decomposition of the stored energy function is then

$$W(\mathbf{C}) = \kappa U(J) + \tilde{W}(\mathbf{C}), \tag{4}$$

where κ denotes the bulk modulus and J is the Jacobian of the deformation gradient $\mathbf{F}$. This decomposition implies that the second Piola–Kirchhoff stress is of the form

$$\mathbf{S} = 2\frac{\partial W(\mathbf{C})}{\partial \mathbf{C}} = 2\kappa U'(J)\cdot\frac{\partial J}{\partial \mathbf{C}} + 2\frac{\partial \tilde{W}(\mathbf{C})}{\partial \mathbf{C}}, \tag{5}$$

where $U'(J) = \partial U(J)/\partial J$ and $\partial J/\partial \mathbf{C} = 1/2 \cdot J\mathbf{C}^{-1}$. Let

$$p = \kappa U'(J); \tag{6}$$

then the second Piola–Kirchoff stress tensor $\mathbf{S}$ can be further expressed as

$$\mathbf{S} = pJ\mathbf{C}^{-1} + 2\frac{\partial \tilde{W}(\mathbf{C})}{\partial \mathbf{C}}. \tag{7}$$

3. Stabilized mixed displacement–pressure formulation

Following standard Galerkin procedure, the strong form in Eq. (1) is integrated with a kinematically admissible weighting function $\mathbf{w}^*$

$$\int_B \mathrm{Div}\,(\mathbf{FS})\cdot\mathbf{w}^*\,\mathrm{d}V = \mathbf{0}. \tag{8}$$

In this work, a simple Petrov–Galerkin formulation following that presented in [6] is used. Specifically, following the standard Galerkin method, the strong form of the equilibrium equation in Eq. (1) is integrated with weight function $\mathbf{w}^*$ lying in the kinematically admissible space $W = V \times P$:

$$\mathbf{w}^* = \mathbf{u}^* + \delta\mathbf{F}^{-\mathrm{T}}\nabla p^*, \tag{9}$$

where $\mathbf{u}^*$ is the standard part and the second term is the perturbation, which gives rise to the stabilization term. The coefficient δ is the mesh dependent stabilization coefficient, which is chosen following [1] as $\delta = \alpha h_{\mathrm{e}}^2/2\mu$, where h_{e} is a characteristic element length for element e, α is a non-dimensional, non-negative stability parameter, and μ is the local shear modulus.

Furthermore, let the perturbation term be evaluated elementwise. Then Eq. (8) becomes

$$\int_B \mathrm{Div}\,(\mathbf{FS})\cdot\mathbf{u}^*\,\mathrm{d}V + \sum_{e=1}^{n_{\mathrm{el}}}\int_{B^{\mathrm{e}}}\frac{\alpha h_{\mathrm{e}}^2}{2\mu}\mathrm{Div}\,(\mathbf{FS})\cdot(\mathbf{F}^{-\mathrm{T}}\nabla p^*)\,\mathrm{d}V = 0. \tag{10}$$

The first term in Eq. (8) is now integrated by parts. After introducing the volumetric stress component, p (see Eq. (7)) as an independent variable, and adding Eq. (6) for p we can define the standard mixed finite element formulation for finite hyperelasticity. Find $(\mathbf{u}, p) \in V \times P$ such that for all $(\mathbf{u}^*, p^*) \in V \times P$

$$\begin{aligned}
&\int_B 2\frac{\partial\tilde{W}(\mathbf{C})}{\partial\mathbf{C}} : \left[\mathbf{F}^{\mathrm{T}}\nabla\mathbf{u}^*\right]\mathrm{d}V + \int_B 2p\frac{\partial J(\mathbf{u})}{\partial\mathbf{C}} : \left[\mathbf{F}^{\mathrm{T}}\nabla\mathbf{u}^*\right]\mathrm{d}V \\
&\quad = L_{\mathrm{ext}}(\mathbf{u}^*)\int_B\left(U'(J(\mathbf{u})) - \frac{p}{\kappa}\right)p^*\,\mathrm{d}V \\
&\qquad - \sum_{e=1}^{n_{\mathrm{el}}}\frac{\alpha h_{\mathrm{e}}^2}{2\mu}\int_{B^{\mathrm{e}}}\left\{2\frac{\partial J(\mathbf{u})}{\partial\mathbf{C}} : [\nabla p\otimes\nabla p^*] + \mathrm{Div}\left[2\mathbf{F}\frac{\partial\tilde{W}(\mathbf{C})}{\partial\mathbf{C}}\right]\cdot\left[\mathbf{F}^{-\mathrm{T}}\nabla p^*\right]\right\}\mathrm{d}V = 0.
\end{aligned} \tag{11}$$

For the above formulation, Klaas et al. [6] have successfully obtained the solution for linear displacement interpolations, in which the higher order derivative, i.e. $\mathrm{Div}\,[2\mathbf{F}(\partial\tilde{W}(\mathbf{C})/\partial\mathbf{C})]$, is zero. However for higher order interpolations, $\mathrm{Div}\,[2\mathbf{F}(\partial\tilde{W}(\mathbf{C})/\partial\mathbf{C})]$, which depends in a complicated way on the gradient of the displacement field, is not zero and must be computed. In this work, a local reconstruction method, following the work presented for two-dimensional Navier–Stokes equations in [7], is used.

We will call the reconstructed term $\mathbf{Q}$, which is $2\mathbf{F}(\partial\tilde{W}/\partial\mathbf{C})$ in Eq. (11). The divergence of the reconstructed term $\mathbf{Q}$ can be expressed in terms of the element shape functions and the node quantities as

$$\frac{\partial Q_{ij}}{\partial x_j} = \sum_{a=1}^{n} N_{a,j}\hat{Q}_{aij} \quad (j = 1,2,3), \tag{12}$$

where N_a are shape functions and $\hat{Q}_{aij}$ is the reconstructed tensor with components ij at node a. This term can be reconstructed to be a continuous variable using an L_2 projection operator performed for each element in a local sense

$$\int_{B^{\mathrm{e}}} N_a N_b\,\mathrm{d}V\hat{\mathbf{Q}}_b = \int_{B^{\mathrm{e}}} N_a\mathbf{Q}\,\mathrm{d}V, \tag{13}$$

where a and b refer to the element nodes.

Furthermore, to avoid computing the more complex derivatives needed for linearization in the Newton–Raphson solution scheme, we move the last term in Eq. $(11)_2$ over to the right-hand side and treat it as a force term, i.e.

$$\int_B\left(U'(J(\mathbf{u})) - \frac{p}{\kappa}\right)p^*\,\mathrm{d}V - \sum_{e=1}^{n_{\mathrm{el}}}\frac{\alpha h_{\mathrm{e}}^2}{2\mu}\int_{B^{\mathrm{e}}} 2\frac{\partial J(\mathbf{u})}{\partial\mathbf{C}} : [\nabla p\otimes\nabla p^*]\,\mathrm{d}V = \mathscr{F}(p^*), \tag{14}$$

where

$$\mathscr{F}(p^*) = \sum_{e=1}^{n_{\mathrm{el}}} \frac{\alpha h_{\mathrm{e}}^2}{2\mu} \int_{B^{\mathrm{e}}} \mathrm{Div}\left[2\mathbf{F}\frac{\partial \tilde{W}(\mathbf{C})}{\partial \mathbf{C}}\right] \cdot (\mathbf{F}^{-\mathrm{T}}\nabla p^*)\, \mathrm{d}V. \tag{15}$$

It should be noted that the term $\mathscr{F}(p^*)$ is reconstructed to be a continuous variable, in a local sense, using an L_2 projection operator performed for each element. The divergence of the reconstructed term can then be expressed in terms of the element shape functions and the node quantities. While this procedure causes the linearization to be inexact because it ignores the dependence of $\mathscr{F}(p^*)$ on the displacement field, it reduces and simplifies the computations in each iteration, and the convergence does not appear to be adversely affected.

4. Linearization

Now Eq. (11), after the local reconstruction (Eq. (14)), can be rewritten in a short form as

$$\begin{aligned} R_{(\mathbf{u},p)}(\mathbf{u}^*) &= L_{\mathrm{ext}}(\mathbf{u}^*), \\ S_{(\mathbf{u},p)}(p^*) &= \mathscr{F}(p^*). \end{aligned} \tag{16}$$

Linearization of Eq. (16), leads to the stabilized system equations

$$\begin{aligned} k_{(\mathbf{u},p)}(\Delta\mathbf{u},\mathbf{u}^*) + g_{(\mathbf{u})}(\Delta p,\mathbf{u}^*) &= L_{\mathrm{ext}}(\mathbf{u}^*) - R_{(\mathbf{u},p)}(\mathbf{u}^*), \\ h_{(\mathbf{u},p)}(\Delta\mathbf{u},p^*) + d_{(\mathbf{u})}(\Delta p,p^*) &= \mathscr{F}(p^*) - S_{(\mathbf{u},p)}(p^*), \end{aligned} \tag{17}$$

where

$$\begin{aligned} k_{(\mathbf{u},p)}(\Delta\mathbf{u},\mathbf{u}^*) = {} & \int_B 4\left[\mathbf{F}^{\mathrm{T}}\nabla(\Delta\mathbf{u})\right]^{\mathrm{sym}} : \left[\frac{\partial^2 \tilde{W}(\mathbf{C})}{\partial\mathbf{C}\,\partial\mathbf{C}} + p\frac{\partial^2 J(\mathbf{u})}{\partial\mathbf{C}\,\partial\mathbf{C}}\right] : \left[\mathbf{F}^{\mathrm{T}}\nabla\mathbf{u}^*\right]^{\mathrm{sym}} \mathrm{d}V \\ & + \int_B 2\left(\frac{\partial \tilde{W}(\mathbf{C})}{\partial\mathbf{C}} + p\frac{\partial J(\mathbf{u})}{\partial\mathbf{C}}\right) : \left[\nabla(\Delta\mathbf{u})^{\mathrm{T}}\nabla\mathbf{u}^*\right] \mathrm{d}V, \\ g_{(\mathbf{u})}(\Delta p,\mathbf{u}^*) = {} & \int_B 2\Delta p\frac{\partial J(\mathbf{u})}{\partial\mathbf{C}} : \left[\mathbf{F}^{\mathrm{T}}\nabla\mathbf{u}^*\right] \mathrm{d}V, \end{aligned}$$

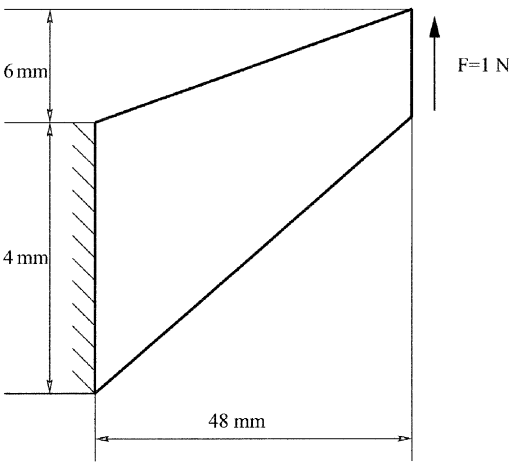

Fig. 1. Cook's plane strain model.

$$h_{(\mathbf{u},p)}(\Delta\mathbf{u},p^*) = \int_B 2p^* U''(J(\mathbf{u}))\frac{\partial J(\mathbf{u})}{\partial \mathbf{C}} : \left[\mathbf{F}^{\mathrm{T}}\nabla(\Delta\mathbf{u})\right] \mathrm{d}V - \sum_{e=1}^{n_{\mathrm{el}}} \frac{\alpha h_{\mathrm{e}}^2}{2\mu} \int_B 4[\nabla p \otimes \nabla p^*]^{\mathrm{sym}} : \frac{\partial^2 J(\mathbf{u})}{\partial \mathbf{C}\,\partial \mathbf{C}} : \left[\mathbf{F}^{\mathrm{T}}\nabla(\Delta\mathbf{u})\right]^{\mathrm{sym}} \mathrm{d}V,$$

$$d_{(\mathbf{u})}(\Delta p,p^*) = -\int_B \frac{1}{\kappa} p^* \Delta p \,\mathrm{d}V - \sum_{e=1}^{n_{\mathrm{el}}} \frac{\alpha h_{\mathrm{e}}^2}{2\mu} \int_{B^{\mathrm{e}}} 2\frac{\partial J(\mathbf{u})}{\partial \mathbf{C}} : [\nabla(\Delta p) \otimes \nabla p^*] \,\mathrm{d}V.$$

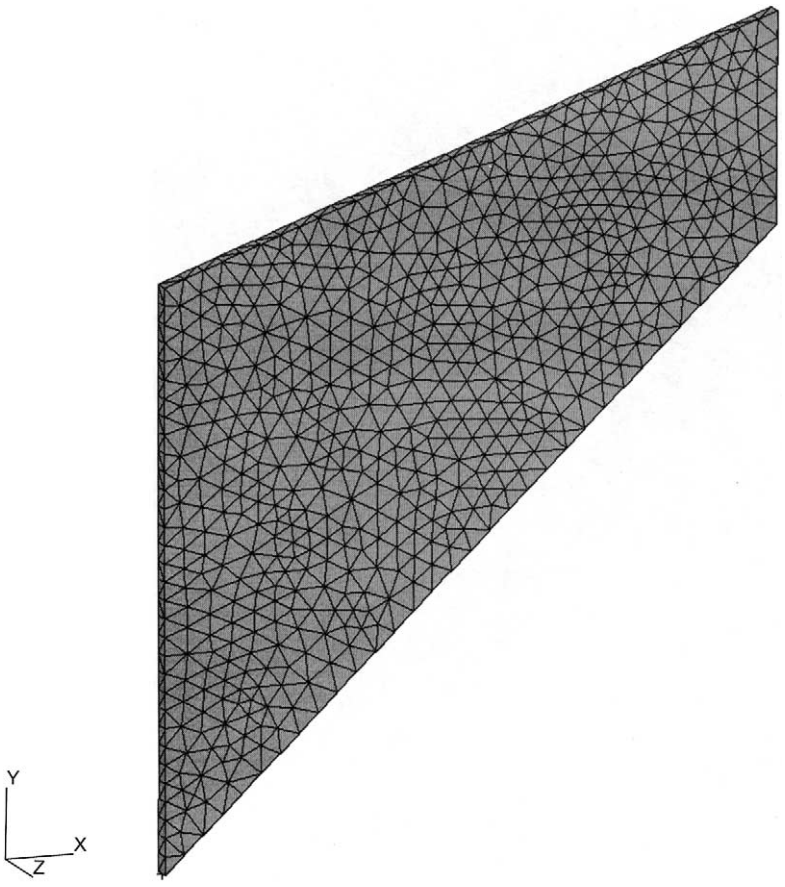

Fig. 2. Mesh (3464 elements) of Cook's model.

Table 1
Principal stress comparison for Cook's problem: Units are N/mm^2, S = stabilized, NS = non-stabilized

Elements	P2/P1	S P1/P1	NS P1/P1	S P2/P2	NS P2/P2	P3/P2
dof	67,320	4968	4968	88,104	88,104	192,024
$\sigma^{\mathrm{I}}_{\min}$	−0.169	−0.15	−0.96	−0.163	−0.132	−0.178
$\sigma^{\mathrm{I}}_{\max}$	0.181	0.20	0.42	0.193	0.185	0.195
$\sigma^{\mathrm{II}}_{\min}$	−0.286	−0.17	−1.06	−0.225	−0.227	−0.245
$\sigma^{\mathrm{II}}_{\max}$	0.0958	0.09	0.40	0.102	0.101	0.103
$\sigma^{\mathrm{III}}_{\min}$	−0.458	−0.45	−1.09	−0.480	−0.385	−0.467
$\sigma^{\mathrm{III}}_{\max}$	0.0351	0.04	0.38	0.0372	0.0405	0.038
RMS error	0.019	0.034	0.57	0.012	0.039	–

5. Examples

The above stabilized formulation has been implemented into an object-oriented finite element framework, named Trellis, developed in the Scientific Computation Research Center at Rensselaer Polytechnic Institute, see [8]. In order to provide a quantitative assessment of the above stabilized, mixed finite element formulation and to demonstrate the behavior of the higher order stabilized mixed method, two examples are investigated: (1) Cook's example, and (2) plane strain extension of a rectangular bar with a flat hole. These are the same examples presented in [6] with linear elements and are thus selected for comparison. Hierarchic shape functions are used. The stability parameter α was set to 1.0 for both examples. Two different types of Neo–Hookian material models are introduced. For both we choose the volumetric contribution to be

$$U(J) = \tfrac{1}{2}(J-1)^2. \tag{18}$$

The remainder of the free energy is taken to be one of the following:

$$\tilde{W}(\mathbf{C}) = -\mu \ln J + \tfrac{1}{2}\mu[\operatorname{tr}\mathbf{C} - 3] \tag{19}$$

or

$$\tilde{W}(\mathbf{C}) = \tfrac{1}{2}\mu[J^{-2/3}\operatorname{tr}\mathbf{C} - 3]. \tag{20}$$

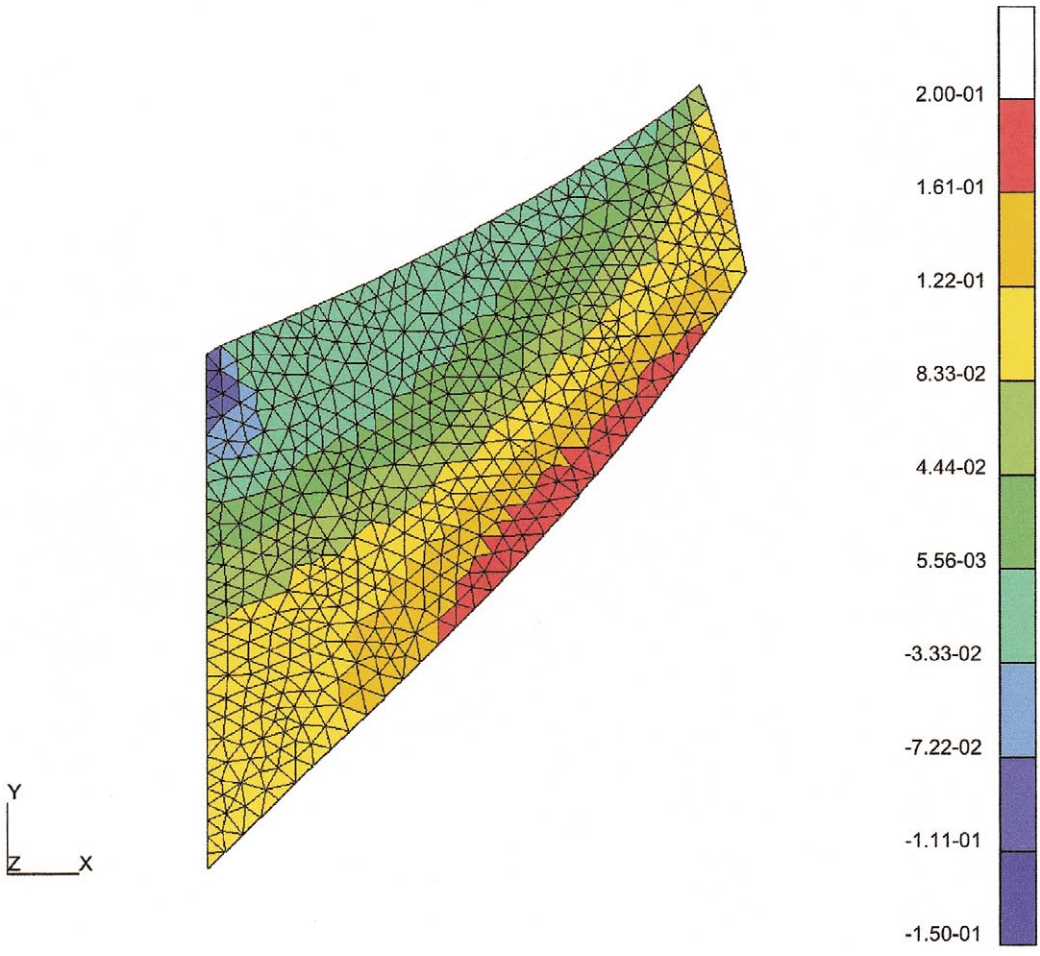

Fig. 3. Cook's model: First principal stress with stabilization (P2/P2 elements).

In Eq. (19), $\tilde{W}$ is not purely isochoric, which can lead to deteriorating results at large strains. The second material model, Eq. (20), is chosen so that $\tilde{W}$ is isochoric. The system relative convergence tolerances in the Newton–Raphson solver are taken to be 10^{-8} for both the examples.

5.1. Cook's plane strain problem

This problem has been used by many authors to test element formulations under combined bending and shear. The model is clamped on one side while it is loaded with a shear load on the other side (Fig. 1). This two-dimensional problem is discretized with a three-dimensional mesh, and the plane strain boundary conditions are applied on the front and back surfaces. The model is discretized with 3464 elements (Fig. 2). The Neo–Hookian material model given in Eq. (19) is used. The materials constants were chosen to be $\kappa = 8000\ \mathrm{N/mm^2}$ and $\mu = 0.8\ \mathrm{N/mm^2}$ which correspond to a Poisson ratio of $\nu = 0.49995$.

Table 1 presents the minimum and the maximum values for the principal stresses that were obtained for different order elements, and Figs. 3–5 show the results for the first principal stress for the P2/P2 and P3/P2 elements. The number of degrees of freedom (dof) that must be solved for, given a fixed mesh, is also listed for each element type in Table 1. For clarification, P1/P1 means linear displacement and pressure interpolation, P2/P1 means quadratic displacement and linear pressure interpolation, etc. Also, non-stabilized solution implies the solution with $\alpha = 0$, and since the P2/P1 and P3/P2 formulations are inherently stable

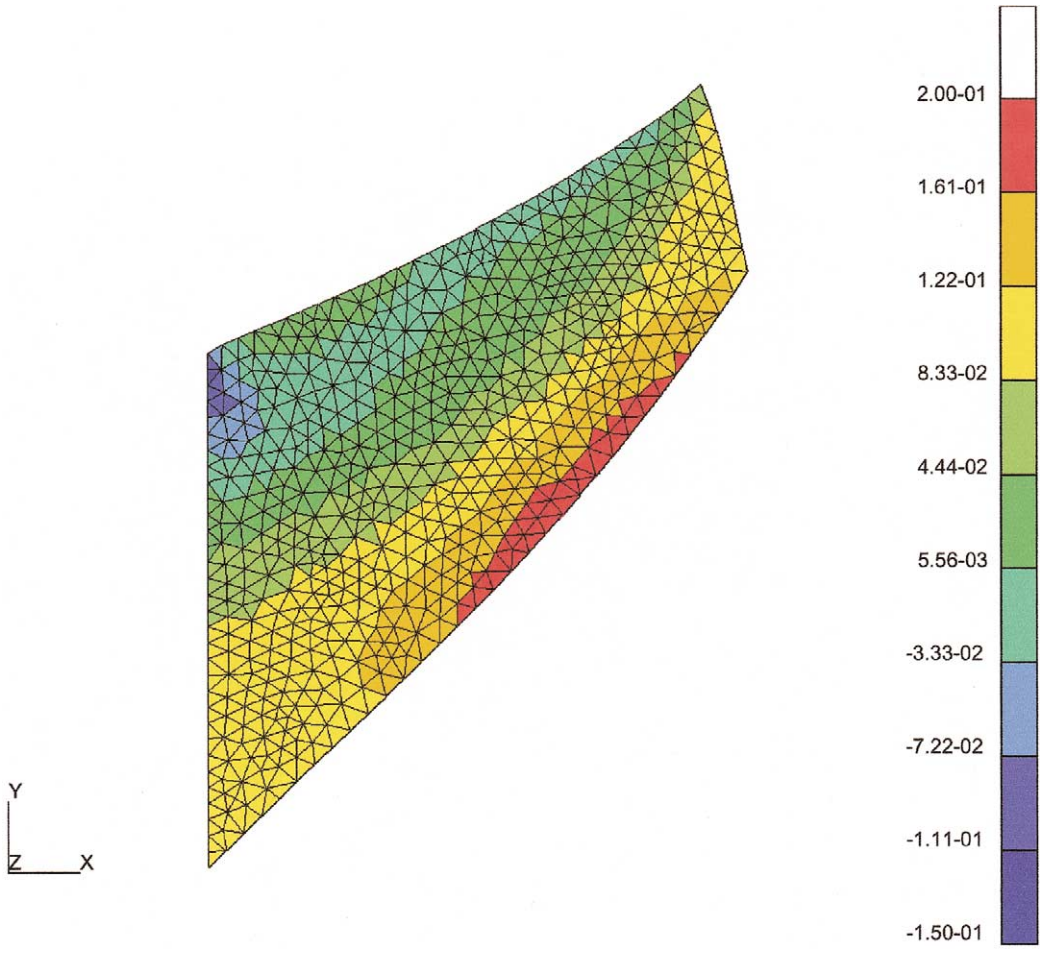

Fig. 4. Cook's model: First principal stress without stabilization (P2/P2 elements).

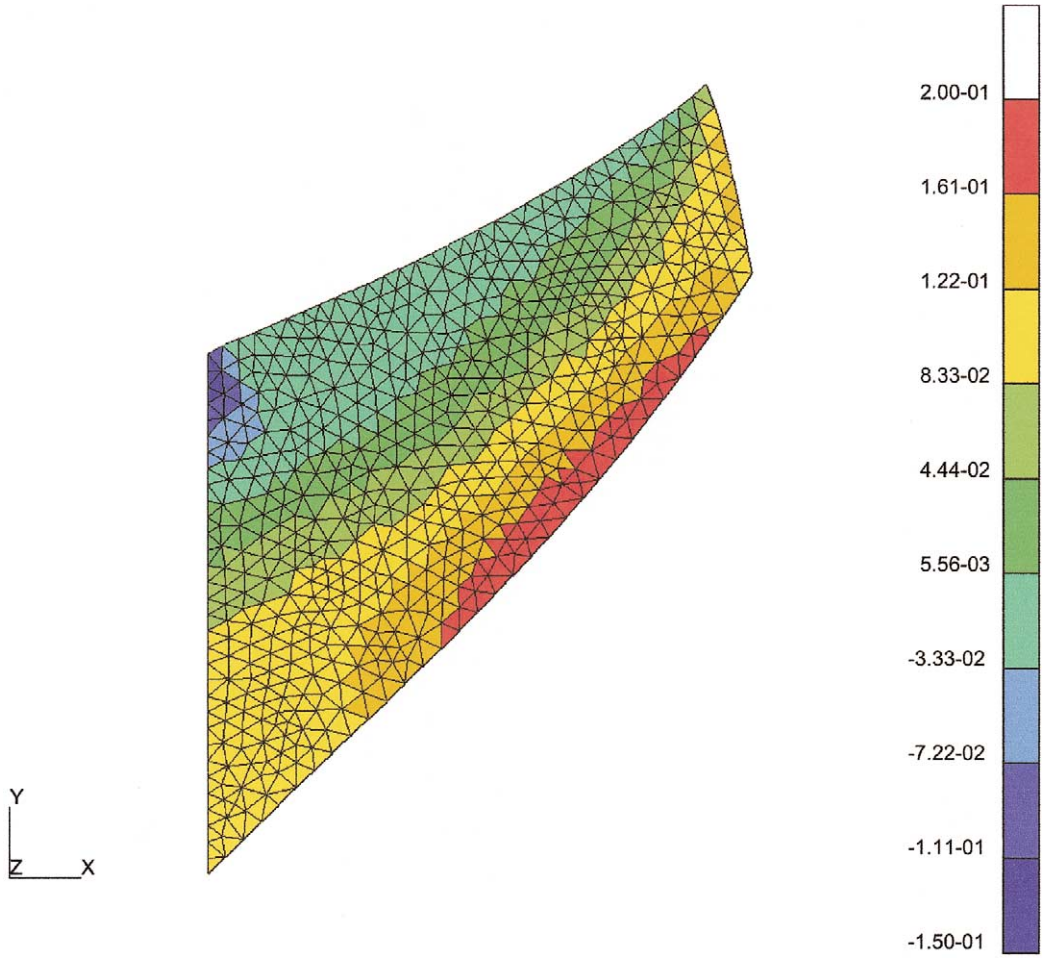

Fig. 5. Cook's model: First principal stress (P3/P2 elements).

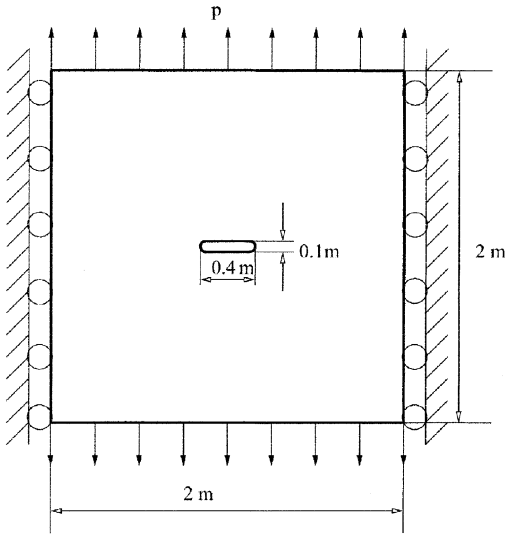

Fig. 6. Plane strain plate model with flat hole.

elements, no stabilization is needed in these cases. Since P3/P2 is a stable element and is the highest order element considered, that solution is assumed to be the most accurate and is used as a reference solution. The root mean square error of the maximum and minimum principal stresses is also listed in Table 1, where the error is defined as the deviation from the P3/P2 element solution. While this does not give an accurate overall error measure, it does pick up extreme values in the solution, which are of interest in detecting unstable behavior in the solution.

From these results, it is apparent that the case with non-stabilized P1/P1 elements gives very poor results. The improvement using the stabilized P1/P1 elements and the significant reduction in degrees of freedom from the P2/P1 case is the most striking result. The stabilized P2/P2 elements give the best results, although they are not significantly better than the results with the P2/P1 elements.

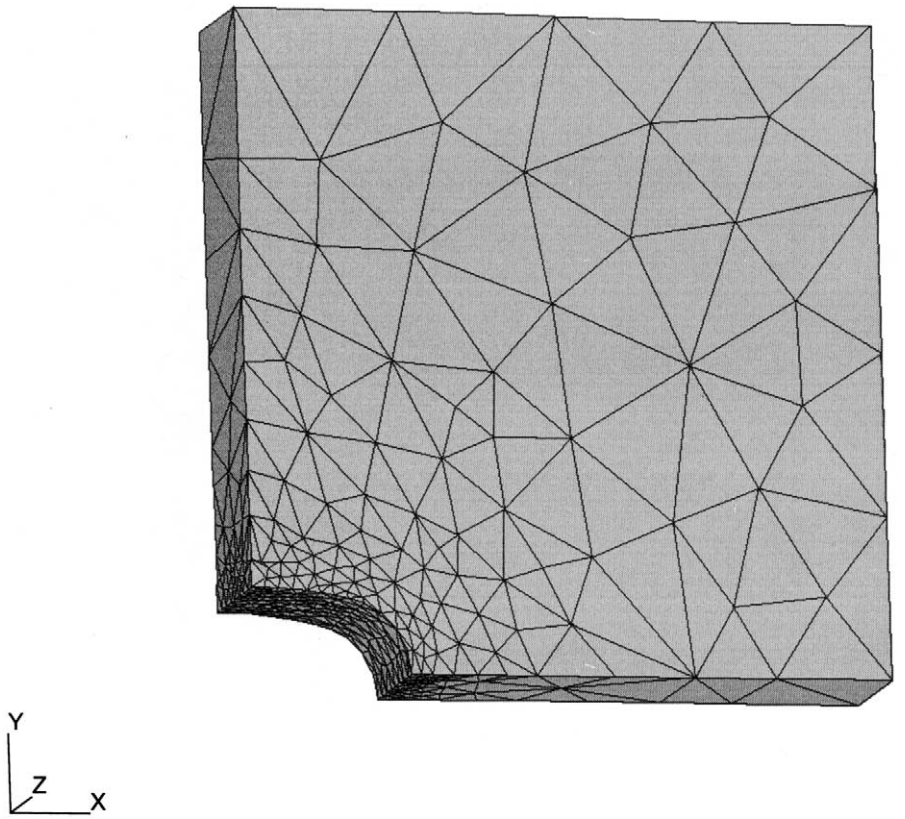

Fig. 7. Mesh (3617 elements) of plate with a flat hole.

Table 2
Principal stress comparison for plate with hole example (1616 elements): Units are N/m^2, S = stabilized, NS = non-stabilized

Elements dof	P2/P1 30,740	S P1/P1 1652	NS P1/P1 1652	S P2/P2 40,436	NS P2/P2 40,436	P3/P2 88,916
σ^{I}_{min}	0.322	0.369	0.301	0.359	0.776	0.320
σ^{I}_{max}	0.745	0.696	1.46	0.696	2.32	0.746
σ^{II}_{min}	0.183	0.313	0.121	0.288	0.776	0.181
σ^{II}_{max}	0.659	0.634	0.967	0.635	1.30	0.650
σ^{III}_{min}	0.00438	0.00497	−0.184	0.00626	0.76	−0.00143
σ^{III}_{max}	0.564	0.576	0.803	0.567	1.08	0.563
RMS error	0.0045	0.062	0.34	0.052	0.85	0.0020

5.2. Plane strain plate with flat hole

Consider a plane strain plate of two by two square meters with a flat hole in the center (Fig. 6). Symmetry and plane strain boundary conditions are applied. A quarter of the plate is modeled using both a course (1616 tetrahedral elements) and a fine (3617 elements) mesh (Fig. 7 shows the fine mesh). The

Table 3
Principal stress comparison for plate with hole example (3617 elements): Units are N/m^2, S = stabilized, NS = non-stabilized

Elements	P2/P1	S P1/P1	NS P1/P1	S P2/P2	NS P2/P2	P3/P2
dof	68,338	3232	3232	90,040	90,040	198,550
σ^{I}_{min}	0.317	0.347	0.310	0.347	0.518	0.318
σ^{I}_{max}	0.747	0.705	1.33	0.704	1.46	0.744
σ^{II}_{min}	0.180	0.247	0.162	0.243	0.438	0.179
σ^{II}_{max}	0.655	0.636	0.902	0.635	1.02	0.652
σ^{III}_{min}	0.003	0.00415	−0.114	0.00311	0.335	−0.00146
σ^{III}_{max}	0.564	0.563	0.820	0.557	0.894	0.566
RMS error	0.0027	0.035	0.28	0.034	0.40	–

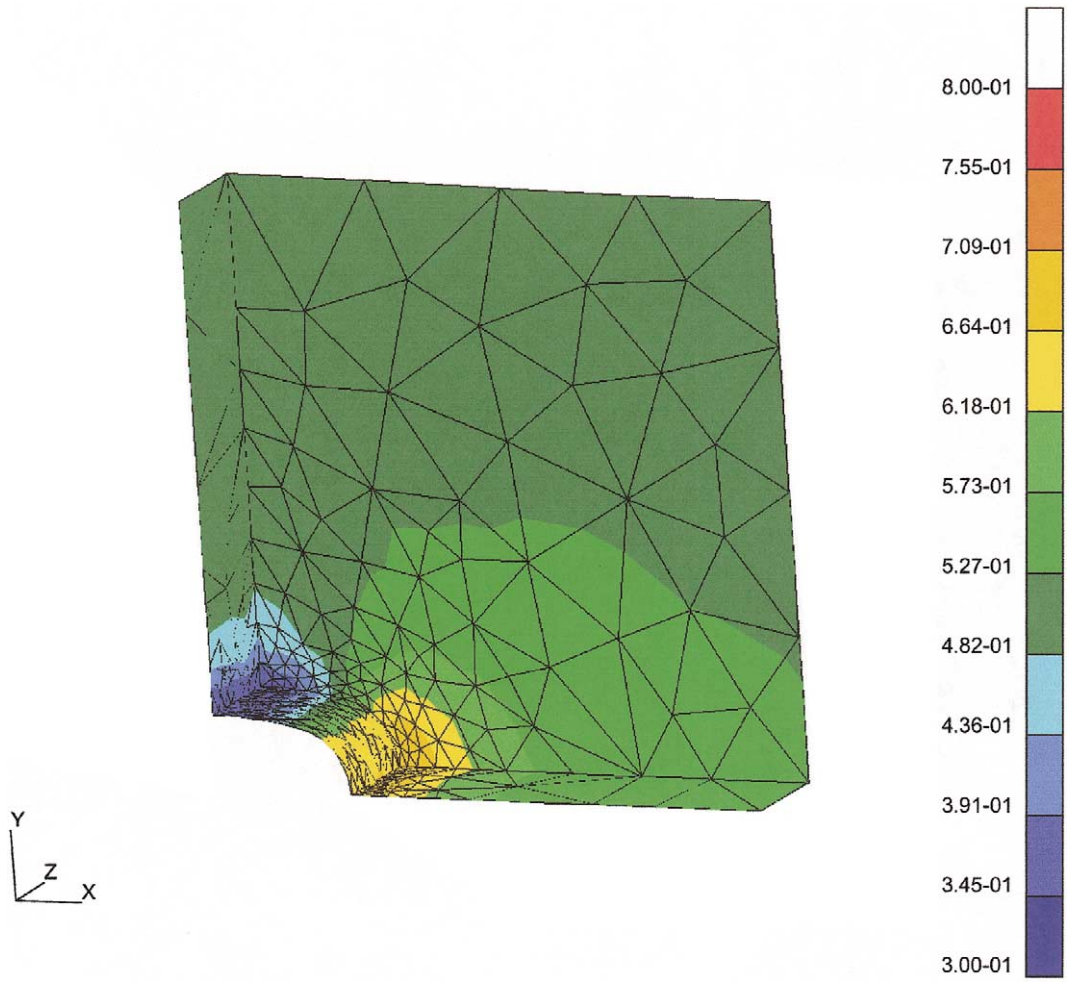

Fig. 8. Plate with hole model: First principal stress with stabilization (P2/P2 elements).

solution is sought for the case with a normal traction boundary condition on the top surface of 0.5 N/m^2. The Neo–Hookian material model given in Eq. (20) is used, and the material parameters are chosen to be $\kappa = 8000\ N/m^2$ and $\mu = 0.8\ N/m^2$.

Tables 2 and 3 present the minimum and the maximum values for the principal stresses that were obtained for different order elements with the coarse and fine meshes, respectively. The number of solution degrees of freedom is also given for each element type. Figs. 8–10 show the solution for the first principal stress using P2/P2 and P3/P2 elements. The root mean square error of the maximum and minimum principal stresses is also listed in Tables 2 and 3, where the error is defined as the deviation from the P3/P2 element solution on the finer mesh. From these results, it is apparent that the cases with non-stabilized P1/P1 and P2/P2 elements give very poor results. It is surprising that the results for the non-stabilized P2/P2 elements is actually worse than that for the non-stabilized P1/P1 elements. It is also interesting to note that although the stabilized P2/P2 element gives a slightly better result than the stabilized P1/P1 element, the result is not as good as for the stable P2/P1 element. The reason for this is likely due to inaccuracies in the reconstructed term **Q**, which is reconstructed locally on an element-by-element basis, and then differentiated (see Eqs. (12)–(15)). To improve accuracy of the higher order element, a more accurate evaluation of the higher order derivative term is probably necessary. However, it should be emphasized that the significant improvement of the stabilized P2/P2 element over the non-stabilized P2/P2 element does demonstrate that the higher order stabilization is effective.

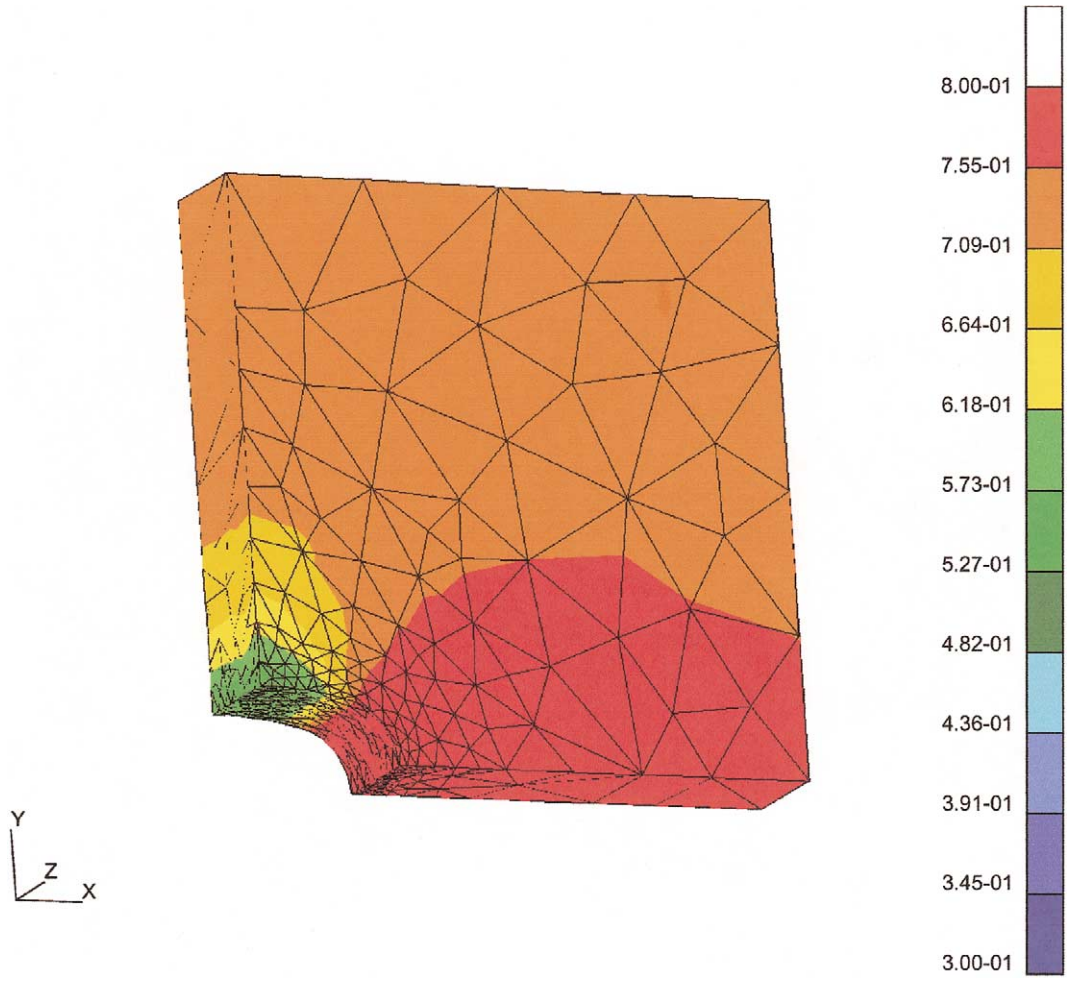

Fig. 9. Plate with hole model: First principal stress without stabilization (P2/P2 elements).

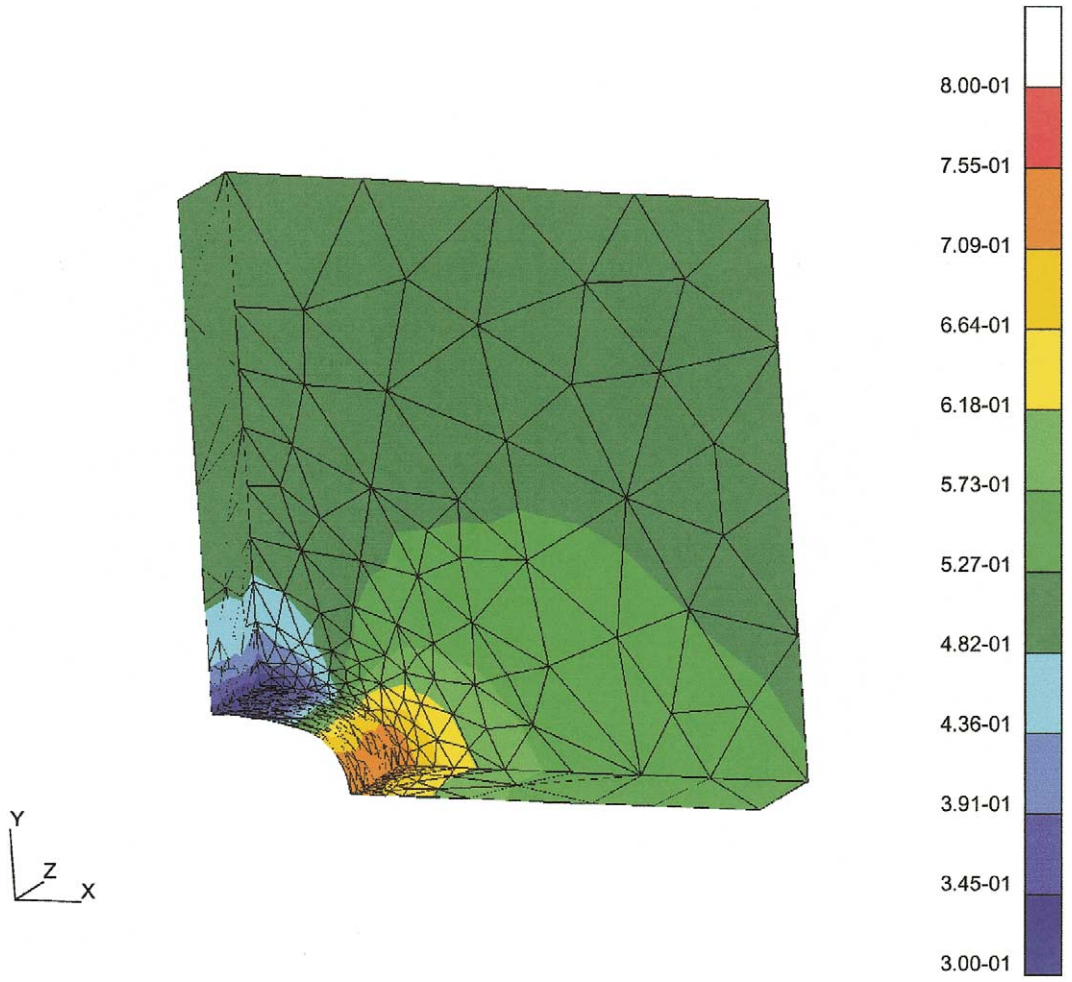

Fig. 10. Plate with hole model: First principal stress (P3/P2 elements).

6. Conclusions

A higher order, stabilized, Lagrangian finite element formulation for nearly incompressible finite deformation hyperelasticity is presented. In the stabilized formulation, mesh dependent terms, which enhance stability, are added element-wise to the usual Galerkin method resulting in a Petrov–Galerkin formulation. A local reconstruction method is used to compute the higher order derivatives that arise in the stabilization terms, specifically derivatives of the stress tensor.

Numerical examples, assuming Neo–Hookian constitutive laws, typical for rubber like materials, are presented in this study. The results demonstrate the effectiveness of the stabilization method for both linear and higher order elements. However, for higher order elements, a more accurate evaluation of the higher order derivative appearing in the stabilization term will be needed to obtain the full benefit of the higher order stabilization. Future work will involve investigating more accurate methods for computing the higher order derivatives in the stabilization and will also focus on extending this work to problems involving finite deformation plasticity.

Acknowledgements

This work has been supported by the National Science Foundation through grant DMI-9634920 as well as by the US Department of Defense – Department of the Air Force, Wright Laboratory.

References

[1] T.J.R. Hughes, L.P. Franca, M. Balestra, A new finite element formulation for computational fluid dynamics: V. Circumventing the Babuska–Brezzi condition: A stable Petrov–Galerkin formulation of the Stokes problem accommodating equal-order interpolations, Comput. Methods Appl. Mech. Engrg. 59 (1985) 85–99.
[2] T.J.R. Hughes, Multiscale phenomena: Green's functions, the Dirichlet-to-Neumann formulation, subgrid scale models, bubbles and the origins of stabilized methods, Comput. Methods Appl. Mech. Engrg. 127 (1995) 387–401.
[3] F. Brezzi, M. Fortin, Mixed and Hybrid Finite Element Methods, Springer, Berlin, 1991.
[4] L.P. Franca, T.J.R. Hughes, A.F.D. Loula, I. Miranda, A new family of stable elements for nearly incompressible elasticity based on a mixed Petrov–Galerkin finite element method, Numer. Math. 53 (1988) 123–141.
[5] J. Douglas, J. Wang, An absolutely stabilized finite element method for the Stokes problem, Math. Comp. 52 (1989) 495–508.
[6] O. Klaas, A.M. Maniatty, M.S. Shephard, A stabilized mixed finite element methods for finite elasticity, Comput. Methods Appl. Mech. Engrg. 180 (1999) 65–79.
[7] K.E. Jansen, S.S. Collis, C. Whiting, F. Shakib, A better consistency for low-order stabilized finite element methods, Comput. Methods Appl. Mech. Engrg. 174 (1999) 153–170.
[8] M.W. Beall, M.S. Shephard, An object-oriented framework for reliable numerical simulations, Engrg. Comput. 15 (1999) 61–72.